

Synaptic Granger Causality: A New Approach to Untangling Excitatory and Inhibitory Connectivities

Víctor J. López-Madrona, Fernanda S. Matias, Claudio R. Mirasso, Santiago Canals and Ernesto Pereda

Abstract—Interactions between brain signals are often measured in terms of information flow. However, when solving the inverse problem—characterizing the structure behind a specific functional link—there are many possibilities with very different consequences. Excitation and inhibition, for instance, may each produce a causal dependence by coordinating neuronal populations, but inhibitory connections do not transmit information packages. Here, we introduce the concept of synaptic Granger causality (sGC), an extension of the well-known Granger causality approach that quantifies the ratio of excitatory/inhibitory projections involved in a functional link on the basis of the analysis of time series constructed using autoregressive models. The method is validated by using the membrane potential obtained from numerical simulations of neuronal motifs that mimic extracellular brain activity, similar to the experimentally measured local field potential. When excitatory and inhibitory synapses are not mixed, the method correctly predicts the type of synapses that participate in the signaling. Moreover, when both inputs project on the same neuron or population, the sGC estimates the proportion of both types of interaction. Our results suggest that sGC allows for a better inference on the anatomical structure underlying effective connectivity and its role in the information process.

Index Terms—Synaptic Granger Causality, Effective Connectivity, Time Series Analysis.

I. INTRODUCTION

THE concept of connectivity in neuroscience is closely related to two main subjects: anatomical and functional networks. The first refers to the physical links between brain structures at different levels, from the synaptic connections

This work was supported by the Spanish Ministerio de Economía y Competitividad (Project Nos. TEC2016-80063-C3-3-R, TEC2016-80063-C3-2-R, and BFU2015-64380-C2-1-R), European Union Horizon 2020 (Grant Agreement No. 668863, SyBil-AA), the Spanish State Research Agency (SEV-2013-0317), the Brazilian Coordenação de Aperfeiçoamento de Pessoal de Nível Superior (Grant Nos. 88881.120309/2016-01 and 88881.068077/2014-01) and the Brazilian Conselho Nacional de Desenvolvimento Científico e Tecnológico (Grant No. 432429/2016-6). E. Pereda would also like to acknowledge the financial support of the University of Ghent as visiting professor at the Department of Data Analysis.

V.J. López-Madrona and S. Canals are with the Instituto de Neurociencias, CSIC-UMH, Sant Joan d'Alacant 03550, Spain (e-mail: v.lopez@umh.es; s.canals@umh.es).

F. Matias is with the Cognitive Neuroimaging Unit, Commissariat à l'Énergie Atomique (CEA), INSERM U992, NeuroSpin Center, 91191 Gif-sur-Yvette, France, on leave from the Instituto de Física, Universidade Federal de Alagoas, 57072-970 Maceió, Alagoas, Brazil (e-mail: fernanda@fis.ufal.br).

C. Mirasso is with Instituto de Física Interdisciplinar y Sistemas Complejos, IFISC (UIB-CSIC), Campus Universitat de les Illes Balears E-07122, Palma de Mallorca, Spain (e-mail: claudio@ifisc.uib-csic.es).

E. Pereda is with Departamento de Ingeniería Industrial, Escuela Superior de Ingeniería y Tecnología, IUNE, Universidad de La Laguna, Tenerife 38205, Spain, and the Laboratory of Cognitive and Computational Neuroscience, CTB, UPM, Madrid, Spain (e-mail: eperpepa@ull.edu.es).

between neurons to the connections between large-scale structures via white matter fiber tracts. However, even if we know every detail of the brain's physiognomy, it remains unclear how the brain processes all the information it receives and its responses to external stimuli [1], [2]. This is the realm of functional connectivity, which studies the statistical relationship between the activities of different areas. Techniques such as electroencephalography and local field potential analysis measure the postsynaptic potential of hundreds of neurons, reflecting the average of their electrical activity. The synchronized spiking of cell assemblies gives rise to oscillations in extracellular recordings [3]–[5] (for example, theta and gamma rhythms in the hippocampus [6], [7]), which have distinct roles. Understanding the rhythms' properties, couplings, and the mechanisms that generate them can have direct clinical benefits, such as in the diagnosis and treatment of patients with epilepsy and other neurological disorders [8], [9].

As an extension of the functionality of brain rhythms, the directionality in their interactions, known as effective connectivity, seems to reflect the pathway of information flow. Studies of causal relationships were initiated by Wiener [10] who hypothesized that if the forecasting of a time-varying signal can be improved by incorporating information from the past values of another signal, then there is a causal influence of the latter on the former. This idea was later implemented by Granger through the use of autoregressive (AR) models, and the method bears his name: Granger causality (GC) [11], [12]. Several methods have been developed since then, based on the same principles, to improve the detection of causal relationships. With partial directed coherence [13], directionality can be computed for each frequency, differentiating between direct and indirect links. The limitations on the detection of only linear relationships were solved using information theory instead of AR models [14]. New tools have also been developed for situations in which the coupling occurs between two different frequencies of the same signal [15].

While it is relatively easy to study statistical relationships between time series of separated regions, it is more difficult to determine information transmission. Analysis of directionality in the connectivity between different physiological structures provides additional information, which helps improve the interpretation of the underlying processes [16]. In the brain, long-range projections are largely based on excitatory synapses, where implications of the information flow can be extrapolated straightforwardly. However, long-range inhibitory projections are also found in many areas [17], quite commonly establishing connections with other inhibitory neurons in the projection fields. While inhibition of postsynaptic targets is

probably not a mechanism suitable for information transmission, these inhibitory projections are likely fundamental in coordinating distant cell populations and facilitating information propagation. Currently, a meaningful characterization of the statistical interdependencies between recorded physiological signals is only possible with detailed knowledge of the anatomical connectivity supporting the system. This is seldom the case in neuroscience. Therefore, we instead propose an extension of the classic GC approach, which we have termed *synaptic Granger causality* (sGC), aimed at inferring the properties of the excitatory/inhibitory ratio in the projections underlying a functional link. This method constitutes a step forward in characterizing the properties of information flow, by taking into account effective connectivity properties (such as directionality) and anatomical constraints (such as excitatory and inhibitory synapses).

In the first section of this paper, we review the concept of GC and present the theory behind the proposed method. We then test and validate our method with time series generated numerically from neuronal models of anatomical motifs in which the structural connectivity is known. Finally, we discuss the advantages and limitations of the sGC and suggest future lines of research in this framework.

II. METHODS

The procedure for calculating the sGC can be divided into two main parts: the estimation of effective connectivity through GC and the measurement of the ratio between positive and negative coefficients of the AR model for those significant networks. As we will show, a positive sGC characterizes an excitatory link, whereas a negative one indicates an inhibitory projection.

A. Granger causality

Given two time series, $X(t)$ and $Y(t)$, it is possible to construct an AR model for each signal in which each time point is the linear combination of their p past samples plus a residual:

$$X(t) = \sum_{k=1}^p A_{1k} X(t-k) + \epsilon_1(t) \quad (1)$$

$$Y(t) = \sum_{k=1}^p A_{2k} Y(t-k) + \mu_1(t) \quad (2)$$

The coefficients in the A matrix represent the weights of the contributions of past values X and Y in the prediction, and ϵ and μ are the residuals (prediction errors). The model order p can be estimated following different criteria, with the Akaike Information Criterion (AIC) [18] and the Bayesian Information Criterion (BIC) [19] being two of the most common choices:

$$AIC = \log(\det(\Sigma)) + \frac{2pn^2}{T} \quad (3)$$

$$BIC = \log(\det(\Sigma)) + \frac{\ln(T)pn^2}{T} \quad (4)$$

where T is the sample size, n is the number of variables and Σ is the covariance noise matrix defined as:

$$\Sigma = \begin{pmatrix} \text{var}(\epsilon) & \text{cov}(\epsilon, \mu) \\ \text{cov}(\mu, \epsilon) & \text{var}(\mu) \end{pmatrix} \quad (5)$$

If we add to (1) the information one of the variables has on the prediction of the other, we obtain a bivariate AR model:

$$X(t) = \sum_{k=1}^p A_{11k} X(t-k) + \sum_{k=1}^p A_{12k} Y(t-k) + \epsilon_2(t) \quad (6)$$

$$Y(t) = \sum_{k=1}^p A_{21k} X(t-k) + \sum_{k=1}^p A_{22k} Y(t-k) + \mu_2(t) \quad (7)$$

If the variance of the error of the bivariate model $\text{var}(\mu_2)$ is smaller than that of the univariate one $\text{var}(\mu_1)$, then the past of $Y(t)$ improves the prediction of $X(t)$; in other words, $Y(t)$ Granger-causes (G-causes) $X(t)$. The model (1) can be extended to the multivariate case by including a set of additional variables $Z_1(t), \dots, Z_k(t)$ whose possible influence on $X(t)$ is also taken into account and eliminated as a confound in $\text{var}(\epsilon_2)$.

Several algorithms and methods can be used to compute GC, including different statistical analyses to check both the AR model and the analysis result [20]–[23]. In this paper, we used the Matlab toolbox proposed by Barnett and Seth [20], where the statistical significance of each value is measured against the null hypothesis of independence using a Wald test [24].

B. Synaptic Granger causality

The second step in determining sGC consists of identifying whether the GCs are due to an excitatory or inhibitory connection between the neural populations represented by $X(t)$ and $Y(t)$. To do that, we have assumed that there is an excitatory link from $Y(t)$ to $X(t)$. This means that an increase in the amplitude of $Y(t)$ leads to an increase in the future values of $X(t)$. In turn, in the case of an inhibitory connection, if there is an increase in $Y(t)$ we can expect a concomitant decrease in the activity of $X(t)$. The idea behind sGC is that this information can be extracted from the coefficients A_{ij} . In fact, we selected those A components that assess the influence of $Y(t)$ to $X(t)$ (A_{12k} , $k = 1, \dots, p$ in (6)). If the average of all k values is positive, we can regard the input from $Y(t)$ as excitatory. If the average of all k values is negative, then the input from $Y(t)$ is regarded as inhibitory.

However, estimating these coefficients is usually not that simple. This is because the data are not clean enough to extract all the correct information, and the time series are too short compared to the optimal model order. Moreover, the algorithms used to solve the equations of (M)AR models tend to assign a value to every A_{ijk} coefficient—even those not improving the forecasting. Here, we propose to estimate which components of the A matrix do not significantly contribute to the AR model, by performing multiple versions of the AR model in (6), deleting all possible combinations of coefficients from the A matrix. The optimum zero constraints are those

belonging to the AR model that minimizes a modified version of the information criteria. One of them is the previous AIC, defined by [25]:

$$AIC' = \log(\sigma^2) + \frac{2m}{T} \quad (8)$$

where σ^2 is the sum of the squared estimation residuals (i.e. ϵ_2, μ_2) divided by the sample size T , and m is the number of estimated parameters. For the original model, the number of parameters for each equation is the model order p multiplied by the number of variables in the model. The total number of matrices with possible zero constraints to test is $2^{(K^2p)} - 1$, where K is the number of variables in the model. As this value is usually too high, we applied two strategies to reduce it: bottom-up followed by top-down [25]:

1) *Bottom-Up Strategy*: Generally, the model order selected is long enough to capture the slowest relationship between the variables considered. However, not all lags provide useful information, for example, when analyzing unconnected nodes. In this case, some type of regularization, which does not include more coefficients than necessary, would be useful. The idea behind this method is to compute the minimum order for the contribution of one time series to the other. Instead of using the whole model, the equation of each variable is analyzed separately. That is, in order to determine the constraints of (6), we will consider the model:

$$X(t) = \sum_{k=1}^{p_{xx}} A_{11k} X(t-k) \quad (9)$$

where p_{xx} is the optimal model, which minimizes the selection criterion. In the next step, p_{xx} is fixed and a new variable is added into the equation, fitting a new order:

$$X(t) = \sum_{k=1}^{p_{xx}} A_{11k} X(t-k) + \sum_{k=1}^{p_{xy}} A_{12k} Y(t-k) \quad (10)$$

Following these steps, a new model order is computed for the participation of one variable to each equation separately, and the coefficients beyond these values are set to zero.

2) *Top-Down Strategy*: Again, we use each variable separately for this method. After setting the excess of coefficients to zero with the previous strategy, the contribution of each remaining value is tested. Initially, we compute the new information criterion value. Then, starting from the furthest nonzero lag, each coefficient is set to zero and the model is estimated again. If the new information criterion is smaller, we update it and keep the zero constraint. If not, both values remain unchanged. For more clarity, considering (6), the first coefficient to test is A_{11p} , then A_{11p-1} and so on.

These strategies allow us to test every single value, considerably reducing the computational cost. Alternative methods can also be applied to determine the constraints of the A coefficients, each with specific advantages and disadvantages (see [25] for details).

Once the linear constraints have been established and the corresponding A coefficients eliminated, we estimate the sGC as the following ratio:

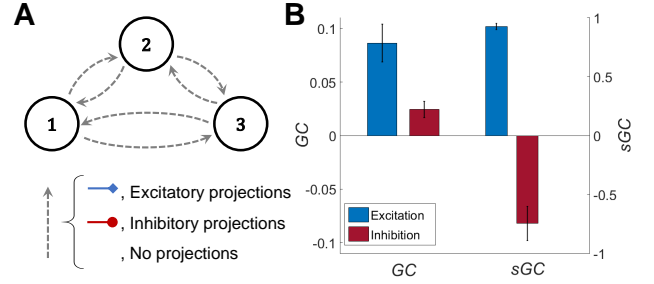


Fig. 1. (A) Scheme of the structure of all implemented motifs. Broken arrows represent the different options for interconnecting the populations that change for each motif. Links can be excitatory, inhibitory or nonexistent. (B) Average of GC and sGC across links, revealing differences in both conditions. Links from an excitatory node exhibit a higher GC and sGC value than those from an inhibitory one.

$$sGC_{ij} = \frac{\sum_{k=1}^p (A_{ijk} > 0)^2}{A_{max_{ij}}} - \frac{\sum_{k=1}^p (A_{ijk} < 0)^2}{A_{max_{ij}}} \quad (11)$$

where the denominator:

$$A_{max_{ij}} = \max \left(\sum_{k=1}^p (A_{ijk} > 0)^2, \sum_{k=1}^p (A_{ijk} < 0)^2 \right) \quad (12)$$

is defined to normalize the index so that $sGC_{ij} \in [-1, 1]$, where $sGC \approx -1$ ($sGC \approx 1$) indicates a dominant inhibitory (excitatory) connection in the link, whereas $sGC = 0$ on a significant link (as assessed by the traditional GC) suggests a balance between excitation and inhibition.

C. Statistical significance

To assess the statistical significance of the method, we tested the null hypothesis that $sGC = 0$. To estimate the sGC distribution, N surrogates ($N = 100$ in this work) were computed by dividing the whole signal into time windows of the same length and selecting a different time reference (i.e. time window) for each channel. In this way, each channel had the same properties as the original signal, but their temporal relation was broken. Next, the normality of the distribution was tested via a Jarque-Bera test and, if it was Gaussian, the associated p-value was established by measuring the distance (in standard deviations) from the sGC value to the mean of the distribution.

D. Neural motifs

To test the validity of our approach, we simulated several neuronal motifs with different structural connectivities. The motifs were composed of three to four nodes connected by chemical synapses, which were either excitatory or inhibitory (see Fig. 2). Each node was a neuronal population composed of 400 excitatory and 100 inhibitory neurons described by the Izhikevich model [26], which receives 50 synapses (sparse connectivity 10%) from randomly selected (excitatory or inhibitory) neighbors in the same population. For the coupling

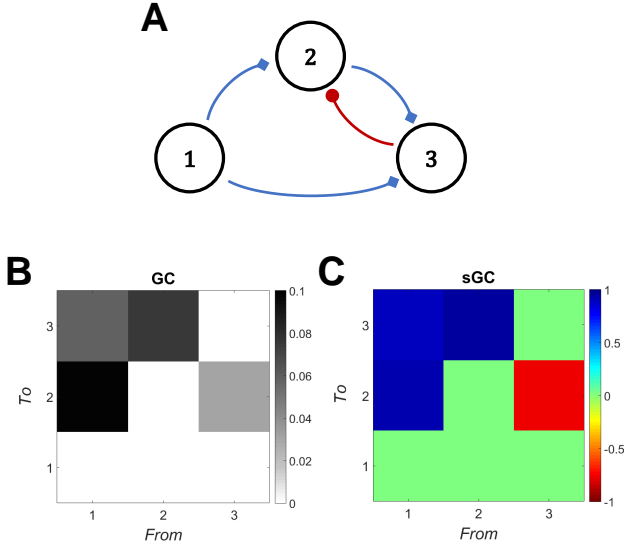


Fig. 2. (A) Representative example of one motif, including three links with excitatory projections (blue arrows) and one with an inhibitory projection (red arrow). (B) GC matrix of the model. All significant values correspond to the implemented structure. (C) sGC ratios for each link, where positive and negative values match excitatory and inhibitory connectivity, respectively.

between the different nodes, we assumed that each postsynaptic neuron receives 20 synapses from presynaptic neurons in the sender population.

The analyzed time series correspond to the mean membrane potential of each population, which is calculated as the average value of the membrane potential v for all neurons within the population. The membrane potential v and the recovery variable u , of each neuron are described by [26]:

$$\frac{dv}{dt} = 0.04v^2 + 5v + 140 - u + \sum I_x \quad (13)$$

$$\frac{du}{dt} = a(bv - u). \quad (14)$$

The summation $\sum I_x$ is over all the synaptic currents. The model establishes that when $v \geq 30$ mV, its value is reset to c and u is reset to $u + d$. The parameters a, b, c and d determine the firing pattern of the neuron. We employ $(a, b) = (0.02, 0.2)$ and $(c, d) = (-65, 8) + (15, -6)\sigma^2$ for excitatory neurons and $(a, b) = (0.02, 0.25) + (0.08, -0.05)\sigma$ and $(c, d) = (-65, 2)$ for inhibitory neurons, where σ is a random variable uniformly distributed on the interval $[0, 1]$ that determines the proportion of different spiking neurons (between regular spiking to bursting modes).

The synaptic current I_x , which can be excitatory, mediated by AMPA (A), or and inhibitory, mediated by GABA_A (G) is described by the following equations:

$$I_x = g_x r_x (E_x - v), \quad (15)$$

where $x = A, G$ and $E_A = 0$ mV and $E_G = -65$ mV are the reversal potentials. Unless otherwise stated all excitatory (inhibitory) weights are set to $g_A = 0.5$ nS ($g_G = 2$ nS).

The dynamics of the fraction of bound synaptic receptors r_x is given by:

$$\tau_x \frac{dr_x}{dt} = -r_x + D \sum_k \delta(t - t_k). \quad (16)$$

The summation over k stands for pre-synaptic neurons. D is taken, without loss of generality, equal to 0.05. The time decays are taken as $\tau_A = 5.26$ ms and $\tau_G = 5.6$ ms. Each neuron is subject to an independent Poisson input, representing n pre-synaptic neurons, with a spiking rate R/n , where $R = 600$ Hz. The Poissonian synapses are assumed as excitatory (AMPA) connections. For each set of parameters we run the simulation for 24 seconds long time series with a sample rate of $Fs = 20$ kHz. For the causality analysis we down sampled the data at 250 Hz. We discard the first 4 seconds to eliminate transient states, until the signal has a *covariance stationary*, i.e. with constant mean and variance.

III. RESULTS

A. Identifying excitatory/inhibitory connections

The first step to validate our approach entailed testing the main assumption underlying sGC, namely, the relationship between the A coefficients of the AR model and the type of projection (excitatory or inhibitory). To do that, we tested 30 motifs composed of three populations (Fig. 1). Maintaining a constant population structure, each motif presented a different connectivity network, where for each link we selected one of three options: only excitatory, only inhibitory or no direct link. Therefore, we expected a positive sGC for those links with excitatory projections and a negative one for those with inhibitory projections. The connectivity of all motifs was set to encompass many different possibilities (Fig. 2), from the simplest case with only one link, to the most complex, with excitatory and inhibitory connectivity among all populations.

When we applied the sGC, the classic effective connectivity was measured by GC analysis (Fig. 1; 100% of hits; excitatory GC: 0.0864 ± 0.0176 ; inhibitory GC: 0.0244 ± 0.0076 ; mean \pm sd), computing the synaptic ratio only in those networks with a significant causality. In summary, 88 links were analyzed (48 excitatory, 40 inhibitory). The results show that sGC differentiates both conditions in all cases (excitatory sGC: 0.926 ± 0.026 ; inhibitory sGC: -0.746 ± 0.145 ; mean \pm sd; $p < 0.05$), which confirms its ability to identify the type of synapses (excitatory or inhibitory) in each of the connections.

B. Determining the excitation/inhibition ratio

We also studied a second type of motif, with four nodes. The results of the sGC again identified the correct causality matrix (Fig. 3), by also identifying the sign of the links in those cases where all the projections are only excitatory or inhibitory. The input from population 2 to population 4 had both types of synapses and, although this link was found, the sGC showed a high positive ratio, suggesting a prevalence of excitation over inhibition.

We then created a modified version of this model by increasing the inhibition in the 2 \rightarrow 4 connection to characterize the ratio of synapses when both types of projection were present in

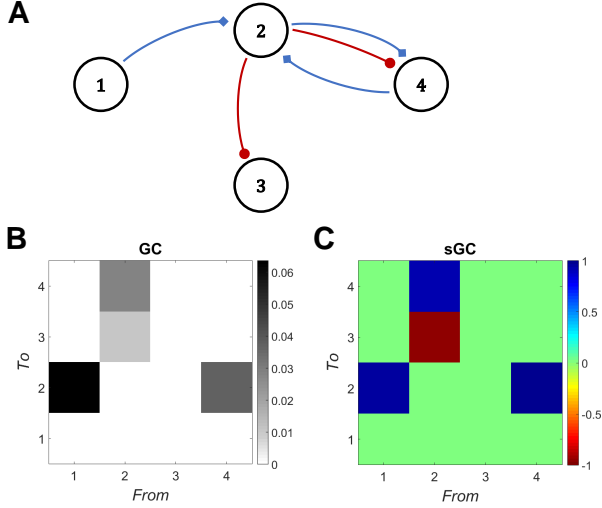


Fig. 3. (A) Scheme of the analyzed motif. Red and blue arrows indicate inhibitory and excitatory projections, respectively. (B) Resulting matrix of GC. Nonzero values represent links with significant causality, which match with the physical network. (C) Matrix with the sGC ratio. Only values with significant sGC are represented ($p < 0.05$). Values near 1 represent predominant excitation; those close to -1 represent higher inhibition. Pairs with a single type of projection (excitatory or inhibitory) are correctly identified, although the projections from population 2 to 4 are considered excitatory, suggesting that excitation is monopolizing the effective connectivity.

the same connection. As the main activity in the original motif was excitatory, the weight of the inhibition was progressively increased while keeping the rest of the parameters constant. The results show a negative trend in sGC in the variable link when the inhibition overcomes the excitation, with the other connectivities remaining stable (Fig. 4). The correlation between the sGC and the inhibitory conductance followed a sigmoidal function, reaching values near the maximum and minimum of the sGC when the inhibition was lower than 2 nS and higher than 4.5 nS, respectively (Fig. 5). The intermediate window can be approximated to a linear regression of both factors ($\rho^2 = 0.92$; $p < 0.0001$; slope $b = -0.75$). In our case, the balance was found for an inhibition weight $g_G \approx 3.25$ nS and $g_A = 0.5$ nS. Thus, as the inhibition increased, the sGC rate became more negative. The projections were identified as predominantly inhibitory for $g_G \geq 5$ nS (sGC = -0.91).

IV. DISCUSSION

We have presented a new GC-based method, sGC, aimed at unraveling further details on the excitatory/inhibitory nature of a functional connection. We successfully tested the sGC for several neuronal motifs, differentiating links based on excitatory and inhibitory projections. sGC allowed us to estimate the existence of the connectivity and provided further insight into the information flow in the system. While the study of functional and effective connectivity reveals how different brain areas connect with each other, what remains unclear is what information is actually transmitted. When determining the type of projections (excitatory or inhibitory) participating in a causal link, positive sGC values indicate successful transmission of information packages, as the activity in the receiver

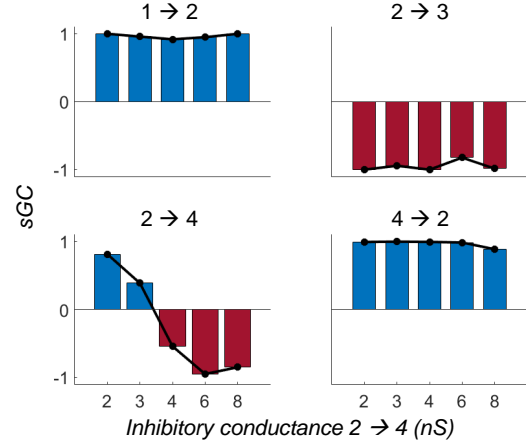


Fig. 4. Evolution of sGC ratio in each link of the motif, as a function of the inhibition weight from population 2 to 4. Changes in the value of this projection only affect the sGC results in that link, while the other links remain the same. An increase in the inhibition weight, involving a change in the excitatory/inhibitory ratio, is captured by our method, showing opposite ratios for inhibition weights of 2 nS and 8 nS (where the excitation is kept constant)

mimics the previous behavior of the transmitter. Conversely, negative values represent the coordination of the different nodes. The number of inputs and outputs of each type to and from a certain region leads to a description of its role in each population.

Furthermore, analysis of a link containing both excitatory and inhibitory synapses revealed differences in their contribution to the measured effective connectivity. For this analysis we balanced the projections to facilitate comparisons, making the inhibitory weights four times greater than the excitatory ones, and the number of inhibitory neurons in each population four times smaller. Under these conditions, however, the causal influence of the excitatory links is still higher (Fig. 1). Also, the interpretation of this result follows the idea of causality as information flow. It is easier to detect than other interpretations of effective connectivity, which could be due to the communication being facilitated by the synchronization of distributed neuronal populations in opportunity time windows.

When both types of projections are present in a link, they compete to control the target population. Our analysis suggests that, in balanced conditions, and for the neuronal dynamic and composition of neural networks used in our models, excitatory activity tends to mask inhibitory activity, as the sGC ratio does not change significantly compared to when only excitatory projections are present (Fig. 3). These results show a correlation between the degree of GC and the type of synapse. However, an increase in the weight of the inhibitory projections changes the sign of the sGC. In fact, as the influence of the inhibition increases to outweigh that of the excitation, there is a progressive decrease in the sGC ratio, until the inhibition dominates in the signal (Fig. 4). This trend also indicates the reliability of the proposed method, as different proportions of projections lead to proportionally smaller values of sGC.

Notwithstanding the promising results obtained with the

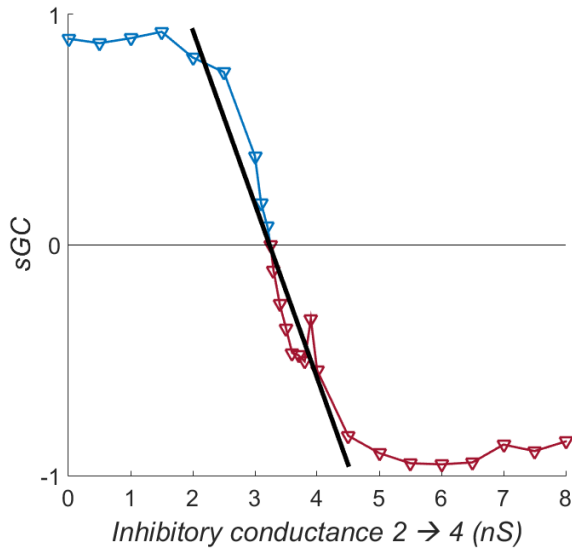


Fig. 5. The sGC ratio presents a sigmoidal behavior in function of the inhibitory conductance, with a working zone of linear correlation (from 2 nS to 4.5 nS).

sGC, there are some limitations. First, to directly interpret sGC in terms of inhibitory or excitatory synapses, there should be a direct anatomical pathway joining the populations. When the connectivity between two points occurs through several areas, we were not able to determine the types of synapses; however, sGC could be used to improve the characterization of that communication. Second, as with any other method used to quantify connectivity, its results are time-dependent, as they are based on the neural activity of the network. The sGC in one link composed of both excitatory and inhibitory projections could change its ratio dynamically as a function of the behavior, showing different processes on the same communication channel. Third, in cases with excitatory and inhibitory projections, it could be possible to separate both conditions as a function of the time delay of their neurotransmitters, so their contribution should be different at different time scales. Nevertheless, the actual spectral variants of GC are not based on the A coefficients of the AR model, so they cannot be characterized following the methodology proposed. Further study of the features of AR models would help overcome these limitations.

REFERENCES

- [1] S. W. Oh, J. A. Harris, L. Ng, B. Winslow, N. Cain, S. Mihalas, Q. Wang, C. Lau, L. Kuan, A. M. Henry *et al.*, "A mesoscale connectome of the mouse brain," *Nature*, vol. 508, no. 7495, p. 207, 2014.
- [2] A. L. Wheeler and A. N. Voineskos, "A review of structural neuroimaging in schizophrenia: from connectivity to connectomics," *Frontiers in human neuroscience*, vol. 8, p. 653, 2014.
- [3] G. Buzsáki, *Rhythms of the Brain*. Oxford University Press, 2006.
- [4] R. T. Canolty, K. Ganguly, S. W. Kennerley, C. F. Cadieu, K. Koepsell, J. D. Wallis, and J. M. Carmena, "Oscillatory phase coupling coordinates anatomically dispersed functional cell assemblies," *Proceedings of the National Academy of Sciences*, vol. 107, no. 40, pp. 17356–17361, 2010.

- [5] C. S. Herrmann, D. Strüber, R. F. Helfrich, and A. K. Engel, "Eeg oscillations: from correlation to causality," *International Journal of Psychophysiology*, vol. 103, pp. 12–21, 2016.
- [6] G. Buzsáki and X.-J. Wang, "Mechanisms of gamma oscillations," *Annual review of neuroscience*, vol. 35, pp. 203–225, 2012.
- [7] L. L. Colgin, "Mechanisms and functions of theta rhythms," *Annual review of neuroscience*, vol. 36, pp. 295–312, 2013.
- [8] P. J. Uhlhaas and W. Singer, "Abnormal neural oscillations and synchrony in schizophrenia," *Nature reviews neuroscience*, vol. 11, no. 2, p. 100, 2010.
- [9] O. Faust, U. R. Acharya, H. Adeli, and A. Adeli, "Wavelet-based eeg processing for computer-aided seizure detection and epilepsy diagnosis," *Seizure-European Journal of Epilepsy*, vol. 26, pp. 56–64, 2015.
- [10] N. Wiener, *Modern mathematics for engineers*. McGraw-Hill, 1956, ch. The theory of prediction.
- [11] C. W. Granger, "Investigating causal relations by econometric models and cross-spectral methods," *Econometrica: Journal of the Econometric Society*, pp. 424–438, 1969.
- [12] S. L. Bressler and A. K. Seth, "Wiener–granger causality: a well established methodology," *Neuroimage*, vol. 58, no. 2, pp. 323–329, 2011.
- [13] L. A. Baccalá and K. Sameshima, "Partial directed coherence: a new concept in neural structure determination," *Biological cybernetics*, vol. 84, no. 6, pp. 463–474, 2001.
- [14] E. Pereda, R. Q. Quiroga, and J. Bhattacharya, "Nonlinear multivariate analysis of neurophysiological signals," *Progress in neurobiology*, vol. 77, no. 1-2, pp. 1–37, 2005.
- [15] H. Jiang, A. Bahramisharif, M. A. van Gerven, and O. Jensen, "Measuring directionality between neuronal oscillations of different frequencies," *Neuroimage*, vol. 118, pp. 359–367, 2015.
- [16] V. J. López-Madrona, F. S. Matias, E. Pereda, S. Canals, and C. R. Mirasso, "On the role of the entorhinal cortex in the effective connectivity of the hippocampal formation," *Chaos: An Interdisciplinary Journal of Nonlinear Science*, vol. 27, no. 4, p. 047401, 2017.
- [17] S. Melzer, M. Michael, A. Caputi, M. Eliava, E. C. Fuchs, M. A. Whittington, and H. Monyer, "Long-range–projecting gabaergic neurons modulate inhibition in hippocampus and entorhinal cortex," *Science*, vol. 335, no. 6075, pp. 1506–1510, 2012.
- [18] H. Akaike, "A new look at the statistical model identification," *IEEE transactions on automatic control*, vol. 19, no. 6, pp. 716–723, 1974.
- [19] G. Schwarz *et al.*, "Estimating the dimension of a model," *The annals of statistics*, vol. 6, no. 2, pp. 461–464, 1978.
- [20] L. Barnett and A. K. Seth, "The mvgc multivariate granger causality toolbox: a new approach to granger-causal inference," *Journal of neuroscience methods*, vol. 223, pp. 50–68, 2014.
- [21] J. Cui, L. Xu, S. L. Bressler, M. Ding, and H. Liang, "Bsmart: a matlab/c toolbox for analysis of multichannel neural time series," *Neural Networks*, vol. 21, no. 8, pp. 1094–1104, 2008.
- [22] G. Niso, R. Bruña, E. Pereda, R. Gutiérrez, R. Bajo, F. Maestú, and F. del Pozo, "Hermes: towards an integrated toolbox to characterize functional and effective brain connectivity," *Neuroinformatics*, vol. 11, no. 4, pp. 405–434, 2013.
- [23] A. K. Seth, "A matlab toolbox for granger causal connectivity analysis," *Journal of Neuroscience Methods*, vol. 186, no. 2, pp. 262–273, 2010.
- [24] A. Wald, "Tests of statistical hypotheses concerning several parameters when the number of observations is large," *Transactions of the American Mathematical society*, vol. 54, no. 3, pp. 426–482, 1943.
- [25] H. Lütkepohl, *New introduction to multiple time series analysis*. Springer Science & Business Media, 2005.
- [26] E. Izhikevich, "Simple model of spiking neurons," *IEEE Transaction on Neural Networks*, vol. 14, no. 6, p. 1569, 2003.